Supplementary Information

Functional Silicon Composite Polymer Electrolyte with Hydrofluoric Acid Scavenging for Quasi-Solid-State Lithium Metal Batteries

Li Zhao [a], Li Yang [a], Yu Cheng [a], Hong Zhang [a], Lulu Du [a], Wei Peng [a], Ahmed Eissa Abdelmaoula [b], and Lin Xu [*acd]

[a] State Key Laboratory of Advanced Technology for Materials Synthesis and Processing, School of Materials Science and Engineering, Wuhan University of Technology, Wuhan 430070, China.

[b] Mining and Metallurgical Department, Faculty of Engineering, Al-Azhar University, Naser City, Cairo 11884, Egypt.

[c] Hubei Longzhong Laboratory, Wuhan University of Technology (Xiangyang Demonstration Zone), Xiangyang 441000, Hubei, China.

[d] Hainan Institute, Wuhan University of Technology, Sanya 572000, China.

* Corresponding Author

E-mail: linxu@whut.edu.cn (Lin Xu)

KEYWORDS: polymer electrolytes, Si nanoparticles, hydrofluoric acid, H2O, interface, lithium metal batteries

1. Experimental section

1.1 Preparation of electrolytes with different content of H_2O for scavenging properties test

Four kinds of solutions were prepared to analyze the HF and H_2O scavenging properties of FCPE. The solutions were prepared by mixing 1.5 ml of fresh base electrolyte (1 M $LiPF_6$ EC/EMC/DMC (1/1/1 by weight)) and different content of water (V_{H_2O}: $V_{base\ electrolyte}$: 0.0%, 0.1%, 0.5%, 1.0%). Each solution was mixed in a glovebox and stored for 24 h.

1.2 Fabrication of electrode

The LFP electrode consisted of LFP, acetylene black, and PVDF binder in a mass ratio of 7:2:1. The active loading of the cathode was 1.2~1.9 mg cm^{-2}. All electrodes were dried at 60 ℃ for 24 h in an oven before cell assembly.

1.3 Battery assembly

Full battery: The 17 mm FCPE was placed on top of the 14 mm lithium sheet, and 30 μL of base electrolyte was added drop-wise. Next, the 10 mm single-sided LFP cathode sheet was layered on top of the FCPE surface, and the 15.8 mm steel sheet was pressed on top to encapsulate the structure.

Li‖Li symmetric cell: A FCPE with a diameter of 17 mm was interposed between two lithium metal sheets with a diameter of 14 mm, followed by the addition of 30 μL base electrolyte to form a Li‖Li symmetric cell.

2. Experimental details

2.1. The source of trace water in the battery

To analyze the source of water in the battery, we first tested the water content of the base electrolyte by Karl Fischer titration. Then, FCPE and LFP were immersed in the base electrolyte for 24 h after being placed for 0.5 h in the air. FCPE has the highest water content after immersion, indicating that FCPE absorbs water in the air. The water content of LFP electrode material increased slightly, suggesting that LFP electrode material also absorbs water in the air.

Table S1. Analysis of trace water in LMB materials.

Scheme	Base electrolyte	Base electrolyte + FCPE	Base electrolyte + LFP
Experimental dosage (g)	0.66	0.69	0.63
Water content (ppm)	35.84	49.19	36.15

The LMB materials were immersed in 2 mL of base electrolyte for 12 h.

Base electrolyte Base electrolyte + FCPE Base electrolyte + LFP

2.2. Hydrolysis products of $LiPF_6$

To analyze the decomposition products of $LiPF_6$, the NMR of the base electrolyte was tested. The NMR spectrum of the base electrolyte shows no characteristic peaks of $PO_2F_2^-$ and HF, indicating that the trace water of the base electrolyte is insufficient for the hydrolysis of $LiPF_6$. However, the NMR spectrum shows the characteristic peak of $PO_2F_2^-$ at -78.37 ppm and -80.38 ppm, and the characteristic peak of HF at -167.46 ppm after H_2O was added to the base electrolyte (V_{H_2O}: $V_{base\ electrolyte}$=0.5%) for 24 h.[1-3] The results indicate that $LiPF_6$ is hydrolyzed with the increase of H_2O content.

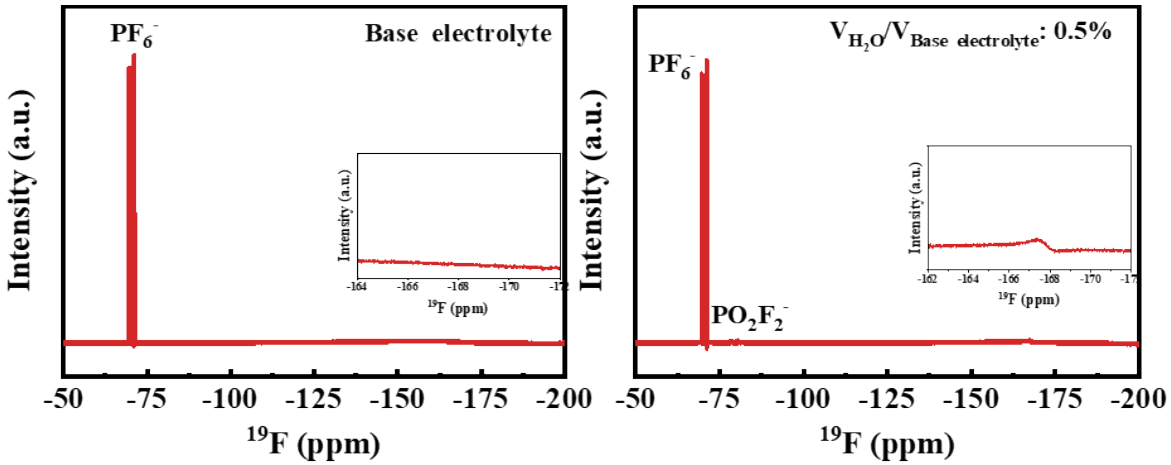

Figure S1. The decomposition of $LiPF_6$ under different conditions. a) ^{19}F NMR spectrum of base electrolytes. b) ^{19}F NMR spectrum of base electrolytes with 0.5% H_2O after storing for 24 h.

2.3. Relative crystallinity of FCPE

Table S2. The degree of relative crystallinity of FCPE.

Samples	T_g [℃]	$T_{m\ PEO}$ [℃]	$\Delta H_{m\ PEO}$ [J g^{-1}]	$T_{m\ PVDF\text{-}HFP}$ [℃]	$\Delta H_{m\ PVDF\text{-}HFP}$ [J g^{-1}]	Relative $X_{c\ PEO}$ [%]	Relative $X_{c\ PVDF\text{-}HFP}$ [%]
CPE	-41.96	39.15	5.46	158.89	45.47	100	100
FCPE	-42.15	41.92	2.56	160.66	44.13	50	97

T_g: The glass transition temperature

T_m: The melting temperature

The formula for calculating crystallinity is as follows:

$$X_c = \frac{\Delta H_{FCPE}}{\Delta H_{CPE}} \times 10 \qquad \textbf{Equatio}$$

Where the X_c is the degree of relative crystallinity, ΔH_{FCPE} is the melting enthalpy of FCPE, and ΔH_{CPE} is the melting enthalpy of CPE.

2.4. Characterization of the FCPE

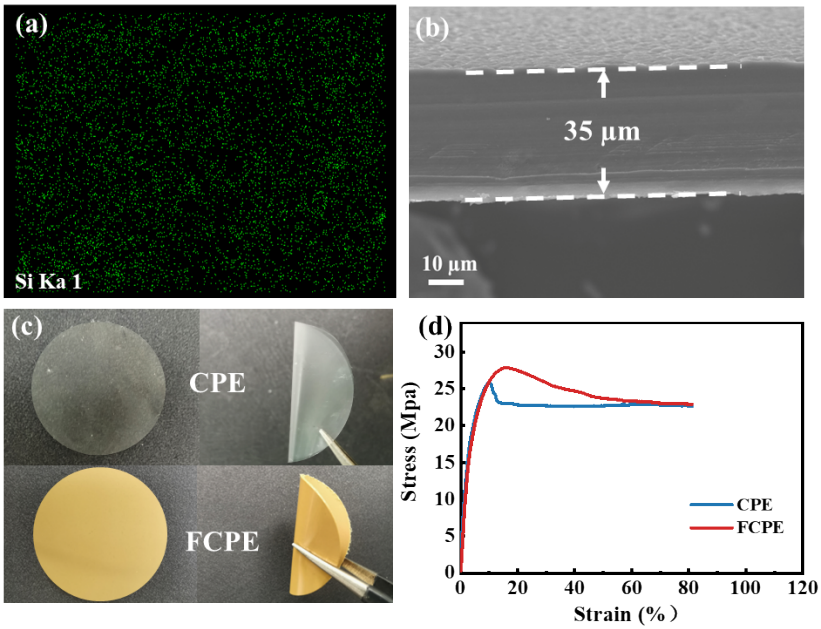

Figure S2. a) EDS mapping of the FCPE. b) Cross-sectional SEM image of the FCPE. c) Photos of the CPE and FCPE in both flat and bent positions. d) Stress-strain curves of CPE and FCPE.

2.5. The effect of Si nanoparticles on composite polymer electrolyte

In the infrared spectrum of FCPE, the peaks at 1401 cm^{-1} and 760 cm^{-1} represent the bending vibration of $-CH_2$, while the peak at 1069 cm^{-1} corresponds to the vibration absorption of −CF.[4, 5] These peaks are characteristic features of the PVDF-HFP α phase. Additionally, the absorption peak at 874 cm^{-1} is a distinctive feature of the PVDF-HFP β phase. The minor peaks observed at 832 cm^{-1} can be attributed to the presence of the PVDF-HFP γ phase. In addition, the C−O−C stretching vibration peak in the infrared spectrum of FCPE appears at 1115 cm^{-1}, while the C−O−C stretching vibration peak appears at 1116.5 cm^{-1} in CPE. The characteristic peaks of PVDF-HFP in FCPE align with those of PVDF-HFP in CPE.[6, 7] However, compared with the CPE, the C−O−C stretching vibration peak of PEO has shifted in FCPE.

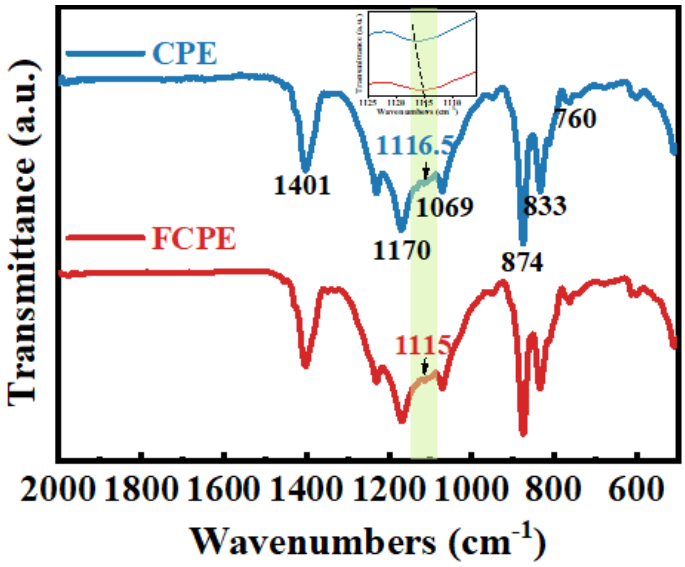

Figure S3. FT-IR spectra of the CPE and FCPE.

2.6. The stability of Si nanoparticles in cells

CV was used to analyze the stability of Si nanoparticles in FCPE cells. The effectiveness of FCPE in protecting Si nanoparticles is shown by the degree of lithiation. As shown in Figure S4, FCPE exhibits similar lithium insertion and delithiation peaks before and after the battery cycle, while no peaks of Si are observed,[8] indicating that the Si nanoparticles in FCPE are well-protected.

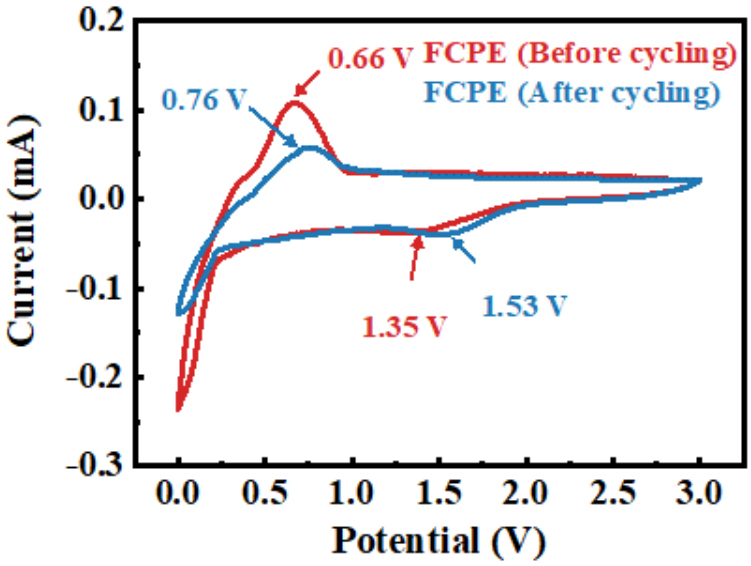

Figure S4. CV curves of FCPE at a scan rate of 0.1 mV s^{-1} at 25 ℃.

2.7. The effect of FCPE on scavenging water

Table S3. Analysis of the effect of FCPE on scavenging water.

Scheme	Base electrolyte	$V_{H_2O}/V_{base\ electrolyte}$-0.1%	$V_{H_2O}/V_{base\ electrolyte}$-0.5%	$V_{H_2O}/V_{base\ electrolyte}$-1.0%
Experimental dosage (g)	0.66	0.50	0.55	0.49
Water content (ppm)	35.84	609.03	687.87	717.40
Experimental dosage (g) (After adding FCPE to the base electrolyte for 24 h.)	0.70	0.54	0.60	0.53
Water content (ppm) (After adding FCPE to the base electrolyte for 24 h.)	34.02	420.15	554.32	712.18

2.8. The content of water after LMB cycling

Table S4. Analysis of water content after LMB cycling.

Scheme	Base electrolyte	Solution after immersing electrode materials
Experimental dosage (g)	0.66	0.61
Water content (ppm)	35.84	34.98

The electrode materials of LMB were immersed in 2 mL of base electrolyte for 12 h.

2.9. The surface composition of FCPE

The composition of the FCPE surface after immersing in electrolytes with varying water content (0.1% H_2O, 0.5% H_2O, and 1.0% H_2O) was analyzed by EDS. The EDS mappings of FCPE show that with an increase in H_2O content, the contents of elements F and Si on the surface of FCPE increased synchronously.

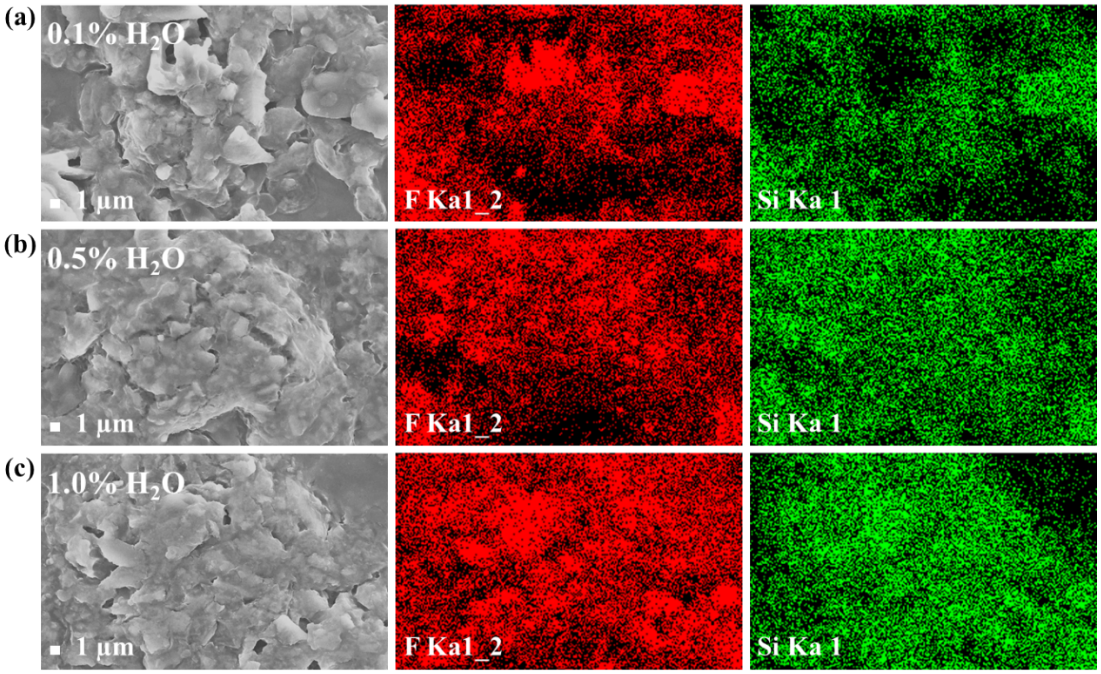

Figure S5. Surface composition analysis of FCPE immersing in electrolytes with varying water content. a)-c) EDS mapping of the FCPE immersing in electrolytes with varying water content (0.1% H_2O, 0.5% H_2O, and 1.0% H_2O).

2.10. The ionic conductivities of FCPE

FCPE was cut into circular plates with a diameter of 17 mm, and its ionic conductivity was measured using EIS with a diameter of 15.8 mm stainless steel electrodes. The test was conducted at frequencies ranging from 10^6 to 1 Hz. The ionic conductivity (σ) was calculated using the following equation:[9-11]

$$\sigma = \frac{L}{RS} \qquad \textbf{Equatio}$$

Where L is the thickness of the FCPE, R is the resistance of the cell obtained from the EIS spectrum, and S is the area of the stainless steel.

Table S5. The ionic conductivities of FCPE.

Scheme	CPE	FCPE
L [μm]	60.00	78.00
R [Ω]	67.00	52.00
r [mm]	15.80	15.80
σ [S cm^{-1}]	4.57×10^{-5}	7.65×10^{-5}

2.11. The lithium-ion transference number

The lithium-ion transference number (t_{Li+}) was obtained from the Li‖Li symmetric cell at 25 ℃ based on Eq.[9, 12]

$$t_{Li+} = \frac{I_{ss}(\Delta V - I_0 R_0}{I_0(\Delta V - I_{ss} R_{ss}} \qquad \textbf{Equatio}$$

Where the ΔV is the polarization voltage, I_0 and R_0 are the current and resistance of the initial state, and the I_{ss} and R_{ss} are the current and resistance of the stable state, respectively. All the electrochemical data were collected by the Autolab PGSTAT302N electrochemical workstation.

Table S6. The transference numbers of lithium ions in CPE and FCPE.

Scheme	CPE	FCPE
R_0 [Ω]	412.00	317.90
R_{ss} [Ω]	422.80	320.80
I_0 [A]	2.31×10^{-5}	2.66×10^{-5}
I_{ss} [A]	1.94×10^{-5}	1.86×10^{-5}
ΔV [mV]	10.00	10.00
t_{Li+}	0.23	0.27

2.12. Fitting results of R_{SEI} of Li‖Li cells assembled with CPE and FCPE

Table S7. Fitting results of R_{SEI} of Li‖Li cells assembled with CPE and FCPE at different temperatures after cycles.

Temperature (℃)	CPE (Ω)	FCPE (Ω)
20	27816.4	4399.8
30	11801.46	1839.917
40	5093.805	1034.887
50	2412.874	593.693
60	1153.844	373.588
70	600.355	230.306
80	334.3	148.713

2.13. Cycling stability of Li‖Li symmetric cells at 0.2 mA cm^{-2}

Li‖Li symmetric cells with FCPEs can cycle stably for 1300 h at the current density of 0.2 mA cm^{-2}, while those with CPEs are shorted after cycling only for 276 h.

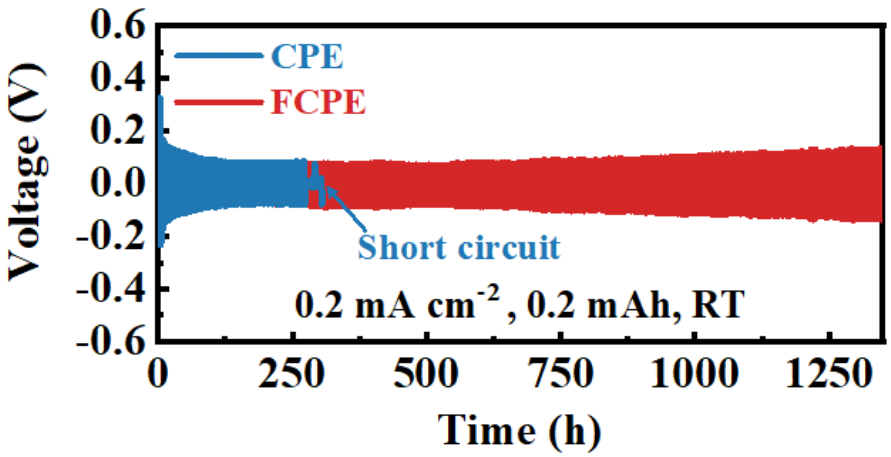

Figure S6. Cycling stability of Li‖Li symmetric cells with FCPEs at the current density of 0.2 mA cm^{-2}.

2.14. The EIS plots of Li‖Li symmetric cells with CPE at different cycles

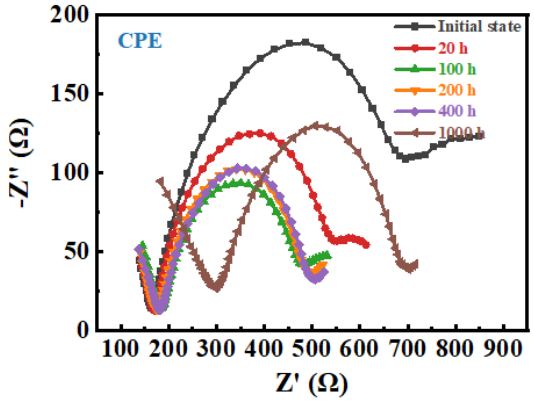

Figure S7 EIS of Li‖Li symmetric cells with CPE at different cycles.

2.15. The cross-sectional SEM images of the lithium metal

The cross-sectional SEM images of the lithium metal in the Li‖Li symmetric cell with CPE after cycling show an uneven interface, while the cross-sectional SEM images of the lithium metal in the FCPE cell reveal a flat interface.

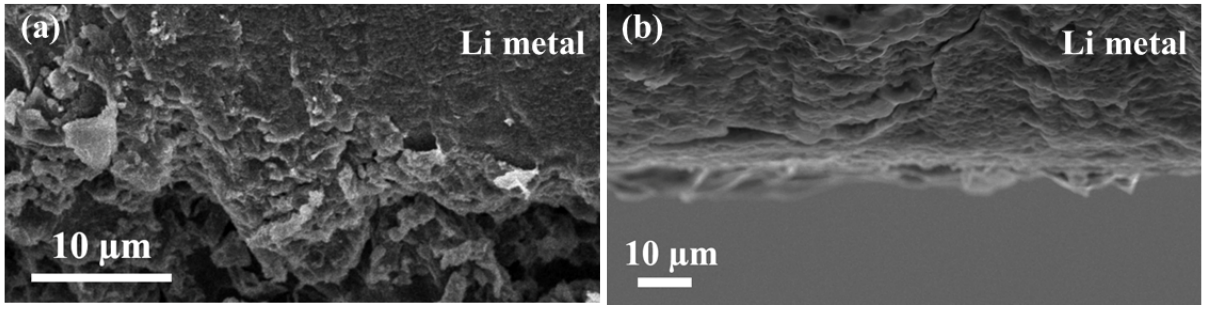

Figure S8. Characterization of the cross-sectional morphology of lithium metal. a) The cross-sectional SEM image of the lithium metal in the Li‖CPE‖Li cell. b) The cross-sectional SEM image of the lithium metal in the Li‖FCPE‖Li cell.

2.16. The component of lithium metal surface after cell cycling

The EDS mapping of the lithium metal shows the density of element F on the surface of lithium metal in the Li‖FCPE‖Li cell is better than that on the surface of lithium metal in the Li‖CPE‖Li cell. It has been shown that the surface of lithium metal may have a LiF-rich SEI layer in the Li‖FCPE‖Li cell.

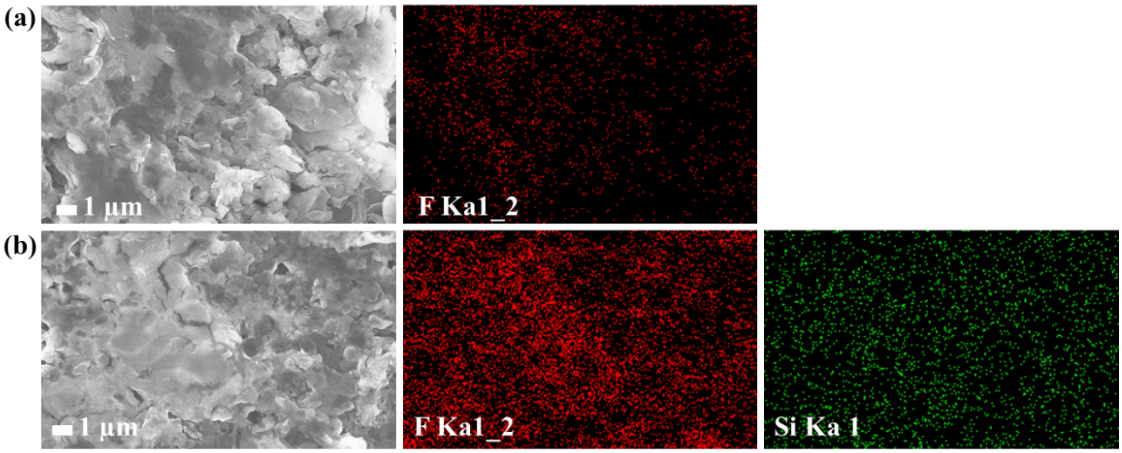

Figure S9. Characterization of the lithium metal surface component after cell cycling. a) EDS mapping of the lithium metal in Li‖CPE‖Li cell. b) EDS mapping of the lithium metal in Li‖FCPE‖Li cell.

2.17. Electrochemical performance of cells with CPE-Li_2SiF_6

Adding 1% Li_2SiF_6 to CPE resulted in the formation of Li_2SiF_6-CPEs. The EIS plots of the Li_2SiF_6-CPEs show that the ionic conductivity was 1.32×10^{-4} S cm^{-1}, whereas the ionic conductivity of the CPE was only 4.57×10^{-5} S cm^{-1} (Figure S10a, Table S8). The cell with CPE containing Li_2SiF_6 can be stably cycled for 1700 h at a current density of 0.1 mA·cm^{-2}. Those results show that Li_2SiF_6 can improve the ionic conductivity of CPE at a certain level. (Figure S10b).

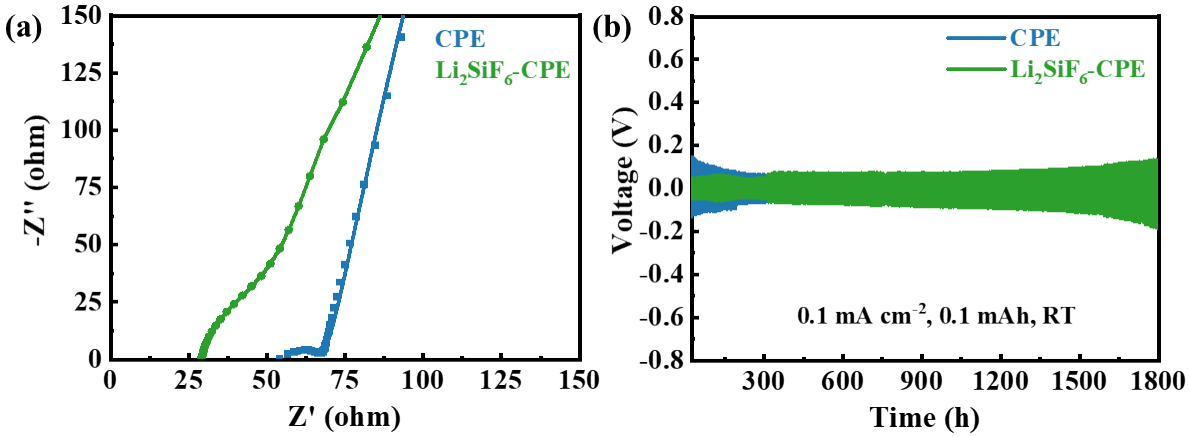

Figure S10. Electrochemical performance of cells with Li_2SiF_6-CPEs. a) EIS plot of the Li_2SiF_6-CPE. b) Cycling stability of Li‖Li symmetric cells with Li_2SiF_6-CPE at a current density of 0.1 mA cm^{-2}.

2.18. The ionic conductivity of CPE-Li_2SiF_6 composite polymer electrolytes

Table S8. The ionic conductivity of Li_2SiF_6-CPEs.

Scheme	CPE	Li_2SiF_6-CPE
L [μm]	60.00	75.00
R [Ω]	67.00	29.00
r [mm]	15.80	15.80
σ [S cm^{-1}]	4.57×10^{-5}	1.32×10^{-4}

2.19. Effect of FCPE on lithium metal surface

A lithium metal sheet was disassembled when the Li‖Li symmetric cell with CPE was cycled to instability. The surface morphology of the lithium metal sheet in the CPE cell was obtained by SEM under inert gas protection. Then, the lithium metal sheet was returned to the glove box with FCPE to assemble a new Li‖Li symmetric cell. The Li‖Li symmetric cells with FCPE can maintain stability for 2000 h at a lower polarization, while those with CPE can remain stable for 1600 h. Compared with the Li‖Li symmetric cell using CPE, the Li‖Li symmetric cell with used lithium metal sheet and FCPE has a more stable cycle. Then, the surface morphology of the same lithium metal sheet was analyzed by SEM. The results show lithium dendrites exist on the lithium metal surface with CPE, while lithium dendrites not be present on the lithium metal surface with FCPE.

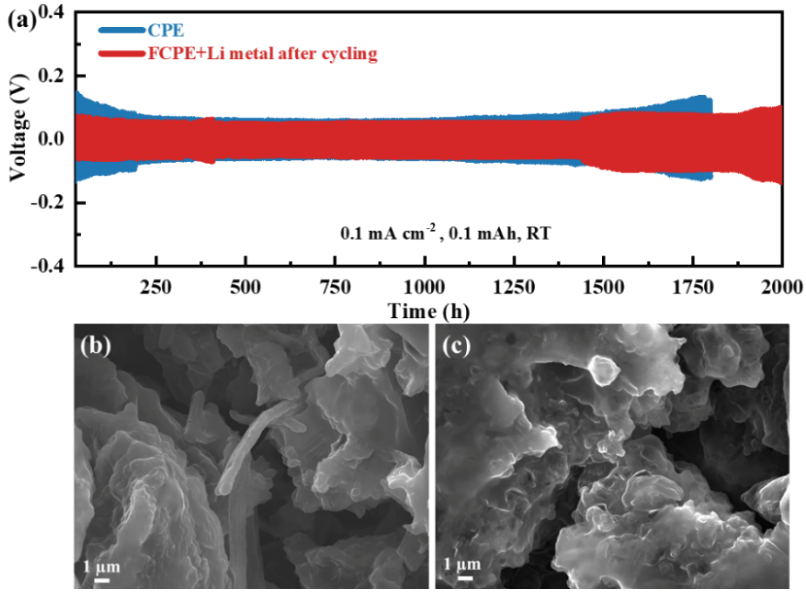

Figure S11. Characterization of the effect of FCPE on the surface of lithium metal. a) Cycling of Li‖Li symmetric cells with CPE and FCPE at a current density of 0.1 mA cm^{-2}. b) SEM image of the lithium metal in the Li‖CPE‖Li cell. c) SEM image of the lithium metal in the Li‖FCPE‖Li cell.

2.20. The composition of lithium metal surface after cycling

The surface morphology of the twice-used lithium metal in the cell with FCPE is uneven, but the Si element is evenly distributed throughout the lithium metal surface. The diffusion of Si in FCPE to the lithium metal surface is difficult. Thus, the uniform distribution of Si elements on the surface of lithium metal may be due to the reaction between Si nanoparticles in FCPE and HF in the cell, which forms gaseous SiF_4 that diffuses onto the surface layer of lithium metal. Then, the SiF_4 reacts with lithium metal and water to form a new SEI layer. Therefore, the EDS mapping of the lithium metal sheet shows the element Si uniform dispersion, indicating the reaction that occurred between the Si and HF.

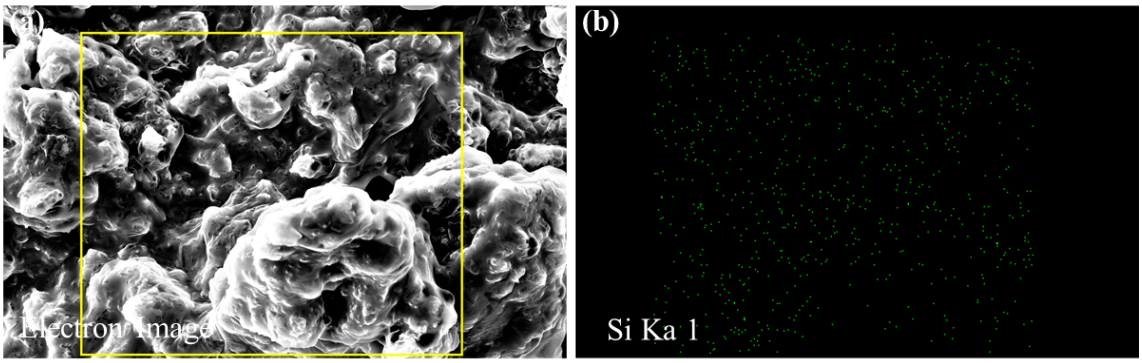

Figure S12. Surface composition analysis of lithium metal in the cell with FCPE after cycling. a) SEM image of the lithium metal surface after recycling. b) The Si elemental EDS mapping of the lithium metal surface after recycling.

References

1 J. P. Allen and C. P. Grey, *J Phys Chem C Nanomater Interfaces*, 2023, **127**, 4425-4438.

2 H. B. Son, S. Cho, K. Baek, J. Jung, S. Nam, D. Y. Han, S. J. Kang, H. R. Moon and S. Park, *Adv. Funct. Mater.*, 2023, **8**, 2302563.

3 B. L. D. Rinkel, D. S. Hall, I. Temprano and C. P. Grey, *J Am Chem Soc*, 2020, **142**, 15058-15074.

4 S. Wu, Z. Yu, X. Nie, Z. Wang, F. Huang and Q. Wei, *Adv. Energy Mater.*, 2022, **12**, 2202930.

5 H. Wang, J. Song, K. Zhang, Q. Fang, Y. Zuo, T. Yang, Y. Yang, C. Gao, X. Wang, Q. Pang and D. Xia, *Energy Environ. Sci.*, 2022, **15**, 5149-5158.

6 Z. Li, Y. Lu, Q. Su, M. Wu, X. Que and H. Liu, *ACS Appl. Mater. Interfaces*, 2022, **14**, 5402-5413.

7 Y. Wei, T. H. Liu, W. Zhou, H. Cheng, X. Liu, J. Kong, Y. Shen, H. Xu and Y. Huang, *Adv. Energy Mater.*, 2023, **13**, e2203547.

8 B. S. Lee, S.-H. Oh, Y. J. Choi, M.-J. Yi, S. H. Kim, S.-Y. Kim, Y.-E. Sung, S. Y. Shin, Y. Lee and S.-H. Yu, *Nat. Commun.*, 2023, **14**, 150.

9 W. J. Hyun, C. M. Thomas, N. S. Luu and M. C. Hersam, *Adv. Mater.*, 2021, **33**, e2007864.

10 X. Fu, M. J. Hurlock, C. Ding, X. Li, Q. Zhang and W. H. Zhong, *Small*, 2022, **18**, e2106225.

11 W. Chen, R. V. Salvatierra, M. Ren, J. Chen, M. G. Stanford and J. M. Tour, *Adv. Mater.*, 2020, **32**, e2002850.

12 M. J. Lee, J. Han, K. Lee, Y. J. Lee, B. G. Kim, K. N. Jung, B. J. Kim and S. W. Lee, *Nature*, 2022, **601**, 217-222.